Spectrochimica Acta Part A: Molecular and Biomolecular Spectroscopy 173 (2017) 439–444

Contents lists available at ScienceDirect

Spectrochimica Acta Part A: Molecular and Biomolecular Spectroscopy

journal homepage: www.elsevier.com/locate/saa

Molecular and structural characterization of some violet phosphate pigments for their non-invasive identification in modern paintings

C. Anselmi [a], M. Vagnini [b], L. Cartechini [a,*], C. Grazia [a,c], R. Vivani [d], A. Romani [a,c,e], F. Rosi [a], A. Sgamellotti [a,c,e], C. Miliani [a,e]

[a] Istituto CNR di Scienze e Tecnologie Molecolari (CNR-ISTM), Via Elce di Sotto, 8, 06123 Perugia, Italy
[b] Associazione Laboratorio di Diagnostica per i Beni Culturali, Piazza Campello 2, 06049 Spoleto, (Perugia), Italy
[c] Dipartimento di Chimica, Biologia Biotecnologie, Università degli Studi di Perugia, Via Elce di Sotto, 8, 06123 Perugia, Italy
[d] Dipartimento di Scienze Farmaceutiche, Università degli Studi di Perugia, Via Fabretti, 48, 06123 Perugia, Italy
[e] Centro di Eccellenza SMAArt, Università degli Studi di Perugia, Via Elce di Sotto, 8, Perugia, Italy

ARTICLE INFO

Article history:
Received 24 September 2015
Received in revised form 22 July 2016
Accepted 17 September 2016
Available online 19 September 2016

Keywords:
Violet phosphate pigments
Non-invasive identification
Near-infrared spectroscopy
UV–Vis
XRD
XRF
Modern paintings

ABSTRACT

A complete non-invasive characterization by XRF, XRD, near-FTIR and UV–Vis reflectance spectroscopy has been performed on some commercially available violet pigments as well as on pure violet Co-salts also known to be used as pigments. The obtained results show that, after a preliminary elemental characterization, the studied pigments can be easily identified by near-FTIR and UV–Vis spectroscopies since they exhibit peculiar spectral bands in these regions. Among the analyzed samples emerged that the pigment 45350 - "Manganviolett" from Kremer consists of two α- and β-$NH_4MnP_2O_7$ polymorphs, being α-$NH_4MnP_2O_7$ the most abundant one; furthermore we found that the pigment R1215D -"Cobalt violet" by Winsor & Newton (no longer available since 2006) displays spectral features that match exactly those of 45820-"Kobaltviolett hell" from Kremer and both are composed by cobalt ammonium phosphate hydrate. Such non-invasive study allowed for the identification of "Manganese Violet" (α-$NH_4MnP_2O_7$) and anhydrous cobalt phosphate ($Co_3(PO_4)_2$) on some Boccioni's paintings during MOLAB *in situ* measurements at the Museo del Novecento (Milano).

1. Introduction

In this work we report a complete non-invasive spectroscopic characterization of six cobalt- and manganese-containing violet pigments carried out within the research activities of a wider ongoing project devoted to investigate futurists' palette and materials [1]. Our interest for such hue arises from its relative recent use as individual pigment since violet nuances in the past were routinely achieved by mixing red and blue pigments and/or dyes.

The first synthetic violet pigment - cobalt phosphate - appeared in late 19th century [2] along with synthetic cobalt arsenate, attempting to reproduce mineral sources (*i.e.* erythrite). Depending on stoichiometry and degree of hydration, cobalt phosphates and arsenates show hues that vary between pink and violet [2]. Over the years manufactures produced different pigment formulations towards less toxic compounds as the Mn-based one, nowadays still available to artists. Manganese violet was first prepared by Leykauf in Germany in 1868 and named "Nuernberg violet" [3]; later it was commercialized by Winsor & Newton as "permanent mauve" in 1892, although the exact pigment composition is somewhat uncertain [4].

The rather fragmented historical sources on pigment formulations motivate the comprehensive spectroscopic study that we undertook to characterize early Co and Mn-based pigments until the contemporary ones. Although some studies for Co-based violet compounds (magnesium cobalt arsenate and hydrate forms, cobalt phosphate and hydrate forms, ammonium cobalt phosphate hydrate, and lithium cobalt phosphate) are known [2,5,6], they have been carried out on samples by means of bench instruments. The complete characterization described in this work deals instead with a non-invasive approach for pigment identification in artworks by portable instrumentation usable *in-situ*, belonging to the mobile laboratory MOLAB [7]. In particular, information from UV–visible spectroscopy, already reported by Corbeil et al. [2] only for the Co-based pigments, has been integrated with near-FTIR spectroscopy analysis and supported by elemental information from X-ray fluorescence and by X-ray diffraction characterization. X-ray diffraction provides unambiguous structural fingerprint for data interpretation of unknown samples. The XRD characterization here supplied can also be utilized directly on site thanks to the recent availability of portable XRD instrumentations for non-invasive investigation of artworks [8,9].

The study was focused on some commercial Co-based pigments from Kremer, some pure Co salts from Aldrich and a no longer available Mn bearing violet pigment from Winsor & Newton.

* Corresponding author.
E-mail addresses: laura.cartechini@cnr.it, laura@thch.unipg.it (L. Cartechini).

http://dx.doi.org/10.1016/j.saa.2016.09.017
1386-1425/

The results highlight that the investigated pigments have distinct spectral signatures making their identification straightforward. This made it possible to identify two Co- and Mn-based violets on some paintings of the Futurist artist Umberto Boccioni (1882–1916) during a MOLAB non-invasive spectroscopic diagnostic session at the *Museo del Novecento* of Milano.

2. Experimental

2.1. Materials and Methods

2.1.1. Pigments

Sources of violet pigments were Kremer (45800, 45820, 45350), Winsor & Newton (R1215D) and Sigma-Aldrich (cobalt lithium phosphate - $LiCoPO_4$, n. 725145, 99% of grade, and cobalt phosphate hydrate - $Co_3(PO_4)_2 \cdot xH_2O$, n. 544140). The powder samples were then analyzed by means of XRF, XRD, UV–Vis reflectance and near-FTIR spectroscopy in a totally non-invasive way. UV–Vis reflectance measurements were carried out on the pigment powders dispersed in white $BaSO_4$.

2.1.2. X-ray Fluorescence (XRF)

XRF spectra were collected using the Bruker ARTAX400. It is equipped with a low-power metal-ceramic-type X-ray tube and a Mo anode as the excitation source which operated at 50 kV and 700 μA. The X-ray fluorescence is revealed by a Peltier-cooled silicon drift detector (SDD) with an active area of 10 mm^2 and a Be window. The typical energy resolution at 5.9KeV is <155 eV. The distance between sample and detector is about 10 mm and the X-ray beam is collimated on the analyzed surface with a spot diameter of 650 μm.

2.1.3. X-ray Diffraction (XRD)

Non-invasive XRD patterns were collected using a *Duetto* XRF/XRD device developed by InXitu, Inc. (Campbell, California) [9,10]. A microfocused X-ray source (Cu, $\lambda = 1.54056$ Å) operating at 30KV with a current of 300 μA is combined with miniature slits to produce a low divergence beam illuminating the sampled surface at 10° incidence angle over an area of 1×0.4 mm^2. A nickel foil mounted on a solenoid motor is placed in the direct beam to remove most of the K_β radiation of the X-ray source spectrum and facilitate the interpretation of XRD data. A custom Peltier cooled CCD camera developed with Andor™ Technology collects the XRD signal as 2D images of sections of diffraction rings over a 2θ range of 20°–50° with a resolution of 0.3°. The XRD analyses were performed in contactless way, maintaining the instrument 2 mm away from the sample surface and using a laser beam for alignment. All components are in a fixed position to guarantee a stable geometry for field applications. Each diffraction pattern consisted of 600 scans corresponding to 1 h 40′ of measuring time.

Bench XRD patterns were recorded with a PANalytical X'PERT PRO diffractometer equipped with a PW3050 goniometer and X'Celerator fast detector. The Ni filtered Cu K_α radiation was used at 40KV and 40 mA. Rietveld refinement analysis was performed with the GSAS program [11].

Phase identification was determined with a search-match program with the help of the ICDD-PDF2 database.

2.1.4. UV–Vis Reflectance Spectroscopy

UV–Vis reflection spectra were recorded by a self assembled instrument composed by an excitation source consisting of a Deuterium-Halogen lamp (Avantes) and a high-sensitivity CCD AvaSpec-2048 (200–1100 nm, Avantes) detector with a spectral resolution of 8 nm equipped with a dedicated optic fiber system [12]. Measurements were carried out with an integration time of 600 ms and 10 averages for each acquisition.

2.1.5. Near-FTIR Spectroscopy

Reflection near-FTIR spectra were recorded using a compact portable JASCO VIR 9600 spectrophotometer equipped with a near-infrared fiber optic sampling probe. The optical bench is made up of a halogen lamp as source, a Michelson interferometer equipped with a CaF_2 beam splitter and a room temperature InGaAs detector. The spectrophotometer is equipped with a Y shaped silica-glass fiber optic probe. In this work, spectra were collected by 200 interferograms covering a spectral range from 14,000 to 4000 cm^{-1}, at a resolution of 8 cm^{-1} and with acquisition times of few minutes. Correction for background absorption was performed by recording the reflectance spectrum of a metal mirror plate as reference. The fiber optic probe was kept perpendicular to the sample surface. The spatial resolution is determined by the probe diameter and is about 4 mm.

3. Results and Discussion

3.1. XRF and XRD

X-ray diffractograms of the violet pigments collected by the portable instrument are illustrated in Fig. 1 while the mineralogical phases identified as well as XRF elemental analysis are reported in Table 1. Since light elements, such as Li and N, are not detectable by XRF, this technique is not able to distinguish among the investigated Co phosphate pigments but the compositional profile of minor elements provides clues for recognition of different commercial formulations. In details, Table 1 shows minor amounts of Mn for 45800 and 45820 (**1** and **2**), both from Kremer, as well as for lithium cobalt phosphate from Aldrich (**4**). In RD1215 from Winsor & Newton (**5**) little amounts of Ba, Sr and a minor content of Sn are present, whilst Aldrich's cobalt phosphate hydrate (**3**) contains Zn and Mn impurities. 45350 from Kremer described as “Manganviolett” (**6**) is composed by Fe, Mn, P and little amounts of

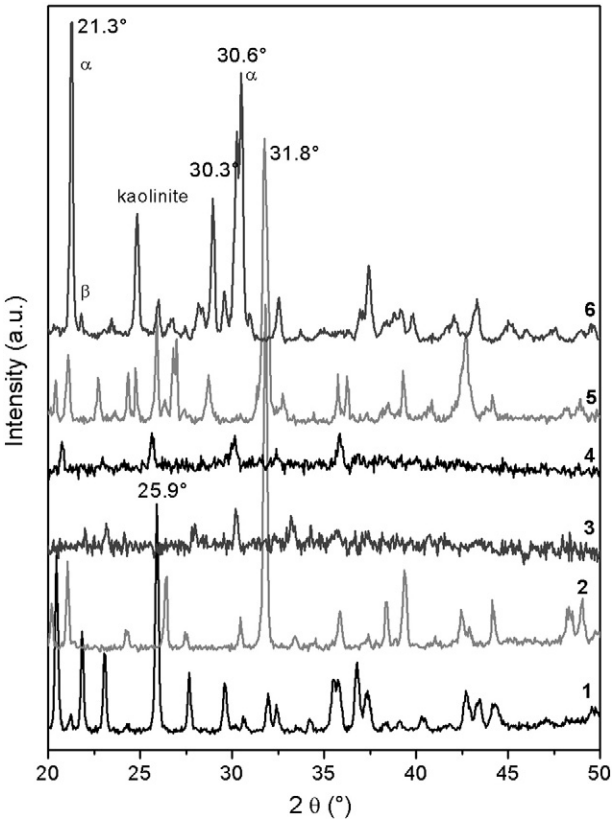

Fig. 1. XRD patterns of the violet pigments collected by the portable X-ray diffractometer. From Table 1, **1** is $Co_3(PO_4)_2$, **2** $NH_4CoPO_4 \cdot H_2O$ from Kremer, **3** $Co_3(PO_4)_2 \cdot 8H_2O$, **4** $LiCoPO_4$, **5** $NH_4CoPO_4 \cdot H_2O$ (with $BaSO_4$) from Winsor & Newton, and **6** $NH_4MnP_2O_7$.

Table 1
Chemical composition by XRF and XRD analysis of the investigated pigments. For XRF results, elements are reported in decreasing order of X-ray fluorescence intensity. Those exhibiting minor signal intensity are indicated in brackets. For XRD results, identified phases and their corresponding reference PDF files (ICDD-number) are reported.

Sample	Commercial name-company	XRF identified elements	XRD identified phase	ICDD Number
1	45800-"Kobaltviolett dunkel"-Kremer	Co, P (Mn)	Cobalt phosphate (monocline)	00-013-0503
2	45820-"Kobaltviolett hell"-Kremer	Co, P (Mn)	Ammonium cobalt phosphate hydrate (orthorhombic)	00-021-0793
3	Cobalt phosphate hydrate-Aldrich	Co, P (Zn, Mn)	Cobalt phosphate hydrate	00-001-0121
4	Lithium cobalt phosphate-Aldrich	Co, P (Mn)	Lithium cobalt phosphate (orthorhombic)	00-032-0552
5	R1215D-Winsor & Newton	Co, Ba, P, Sr (Sn)	Ammonium cobalt phosphate hydrate (orthorhombic)	00-021-0793
			Barite (orthorhombic)	00-024-1035
6[a]	45350-"Manganviolett"-Kremer	Mn, P, Fe, (As, Sr, K)	Ammonium manganese pyrophosphate	
			Kaolinite[b]	01-079-1570
			Stewartite[b]	00-005-0110

[a] Analyzed also by a bench top XRD, see Table 2, Fig. 2 and text for further details;
[b] Minor phase.

As, Sr and K. Mn and Zn are known to be typical impurities of Co-based pigments derived from the metal extraction process. Other elements (Sr in pigment **5** and Fe and K in pigment **6**) may be present as impurities of the pigment accessory phases identified by XRD and discussed below. The remaining elements may have been introduced during the manufacturing process but the low amount (X-ray fluorescence intensities two or three order of magnitude lower than Co or Mn) did not allow verifying their presence as minor compounds or as substitutive elements in the crystalline phases.

From XRD analysis only one phase has been found for **1** – *i.e.* cobalt phosphate, $Co_3(PO_4)_2$ – showing a monocline crystal structure and the most intense signal at $2\theta = 25.9°$. In **2** only cobalt ammonium phosphate hydrate — $NH_4CoPO_4 \cdot H_2O$ — with an orthorhombic structure was detected showing the most intense signal at $2\theta = 31.8°$. Such XRD results for the Kremer cobalt-based pigments are confirmed from literature data [2,5,13] where the diffraction patterns were collected by bench top instruments. Pigments **3** and **4** present very low diffraction intensities due to their poor crystallinity. Sample **3** is compatible with different hydrate forms of cobalt phosphate, $Co_3(PO_4)_2 \cdot xH_2O$, nevertheless spectral features in the mid-infrared spectrum suggest the octahydrate form as the most abundant (mid-FTIR spectra in transmission mode are reported in Fig. SM1 of the Supplementary Material). The XRD pattern of sample **4** matches that of cobalt lithium phosphate ($LiCoPO_4$) in an orthorhombic *Pmnb* crystal system. In **5**, two different mineralogical phases were identified: cobalt ammonium phosphate hydrate ($NH_4CoPO_4 \cdot H_2O$) with an orthorhombic crystal structure and barite ($BaSO_4$). The observation of barite accounts for the detection of traces of Sr (a natural substituent).

Concerning the manganese violet (**6**), it was not possible to carry out phase identification by means of the PDF2 database; then a bench top instrument was necessary in order to expand the investigated 2θ-range down to 5.00° and to perform a Rietveld refinement analysis (Fig. 2). It revealed the presence of α-$NH_4MnP_2O_7$ [14] as the most abundant phase in the sample, but also a very small amount of the β-phase. Both the phases have some of the most intense reflections in the working 2θ-range (20°–50°) of the portable XRD (Table 2) which can be used for their identification in non-invasive studies.

Additionally, the Rietveld analysis clearly showed two important features: first, some relevant intense peaks were not matched by the above phases; secondly, intensities of peaks at 12.38° and 24.91° were not well fitted, although included in the calculated pattern of α-$NH_4MnP_2O_7$. An extensive search and match procedure by combining PDF2 database with the extra peak list and the composition of manganese violet gave indication of the presence of two additional phases: one belonging to the class of metal phosphate hydroxide hydrates, that is stewartite (ref. code: 005-0110), with formula $MnFe_2(PO_4)_2(OH)_2 \cdot 8(H_2O)$ and the other is kaolinite ($Al_2Si_2O_5(OH)_4$). The presence of kaolinite was also confirmed by mid-FTIR spectroscopy (see Supplementary Material). Rietveld analysis gave the following weight composition for sample **6**: α-$NH_4MnP_2O_7$ 79.9(1) %; β-$NH_4MnP_2O_7$ 4.5(1) %; kaolinite 13.3(9) %; stewartite 2.3(5) %. Stewartite, although in very small amount, was found to contribute appreciably to the whole pattern because of some overexpressed diffraction peaks due to strong preferential orientation of (010) planes. Both kaolinite and stewartite may account for the observation of minor amounts of K and Fe at the XRF.

3.2. UV–Vis and near-FTIR

UV–Vis measurements in reflection mode of the powdered compounds in the range 300–700 nm are shown in Fig. 3 (left column), together with the corresponding near-FTIR spectra in the range of 14,300–4000 cm^{-1} (700–2500 nm) (right column); near-infrared band assignment is, then, summarized in Table 3. All spectral data are exempt from any smoothing or spectral processing.

3.2.1. UV–Vis Spectral Range: 300–700 nm

The samples exhibit bands in this spectral region due to *d-d* electronic transitions typical for cobalt (II) and manganese (III) in six-coordination (octahedral symmetry).

Cobalt compounds typically are pink-violet in octahedral geometry while they display a deep blue colour in tetrahedral coordination [14,15]. From the correlation diagram of cobalt (II) in octahedral geometry [16] there are three spin-allowed transitions: ν_1 ($^4T_{1g} \rightarrow {}^4T_{2g}(F)$), ν_2 ($^4T_{1g} \rightarrow {}^4A_{2g}(F)$), and ν_3 ($^4T_{1g} \rightarrow {}^4T_{1g}(P)$), [17]. Only this latter is responsible of for the colour, being ν_1 and ν_2 localized in the near infrared region; in particular, ν_2 is a two electron transition usually showing low band intensity. Transitions to T_1 and T_2 states typically show multiple

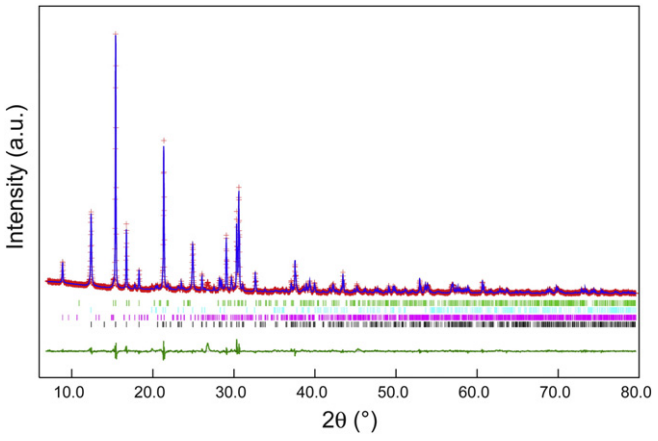

Fig. 2. Rietveld plot for sample **6**, reporting the experimental (red crosses) and the calculated profile (blue curve) along with their difference (green curve). Colour code for peak marks: α-$NH_4MnP_2O_7$ (green); stewartite (cyan); kaolinite (pink); β-$NH_4MnP_2O_7$ (black). Statistical agreement factors: Rwp = 5.56; Rp = 3.93.

Table 2
X-ray powder diffraction data for the first most intense reflections for the α and β phases of $NH_4MnP_2O_7$ identified in sample **6**.

2θ[a]	d (Å)	100 × I/I_{max}	h	k	l
α-$NH_4MnP_2O_7$					
15.398	5.750	100.0	1	1	0
16.723	5.297	29.5	−1	−1	1
21.329	4.163	79.2	0	0	2
29.053	3.071	28.8	1	1	2
30.330	2.945	39.9	1	3	0
30.600	2.919	49.5	−2	−2	1
32.630	2.742	12.2	−1	1	3
37.536	2.394	14.5	−3	−1	1
43.445	2.081	11.8	0	0	4
β-$NH_4MnP_2O_7$					
15.128	5.852	72.8	0	1	0
15.382	5.756	79.6	0	0	1
16.768	5.283	16.7	−1	0	1
17.055	5.195	24.0	−1	1	0
21.748	4.083	16.0	1	−1	1
21.873	4.060	100.0	2	0	0
28.836	3.094	31.6	2	1	0
30.071	2.969	40.5	0	−2	1
30.535	2.925	45.0	−1	0	2

[a] Referred to Cu $K\alpha_1$ radiation (λ = 1.5406 Å).

Table 3
Band assignment in the near-infrared spectral range (4000-14,000 cm^{-1}).

Pigment	Experimental band (cm^{-1})	Band assignment [ref.]
1	4780	*d-d* electronic transition [16,18]
	5870	*d-d* electronic transition [16,18]
	9400	*d-d* electronic transition [16,18]
	11,200	*d-d* electronic transition [16,18]
2 & **5**	4240	Not assigned
	4640	Not assigned
	4845	$(\nu_1 + \nu_4)$ NH_4 [26]
	5000	$(\nu_2 + \nu_3)$ NH_4 [26]
	5095	$(\nu_3 + \nu_2)$ H_2O [23]
	6500	*d-d* electronic transition [17,22]
	13,900	*d-d* electronic transition [19]
3	5090	$(\nu_2 + \nu_3)$ H_2O [23]
	4690	Not assigned
	7300 (broad)	*d-d* electronic transition [17,22]
4	5350	*d-d* electronic transition
	6100	*d-d* electronic transition
	7730	*d-d* electronic transition [19]
	12,750	*d-d* electronic transition [19]
6	4530, 7063	Kaolinite
	4640	$(\nu_1 + \nu_4)$ NH_4 [26]
	4870	$(\nu_2 + \nu_3)$ NH_4 [26]
	6380	$(\nu_1 + \nu_3)$ NH_4 [26]
	11,000	d-d electronic transition [21]

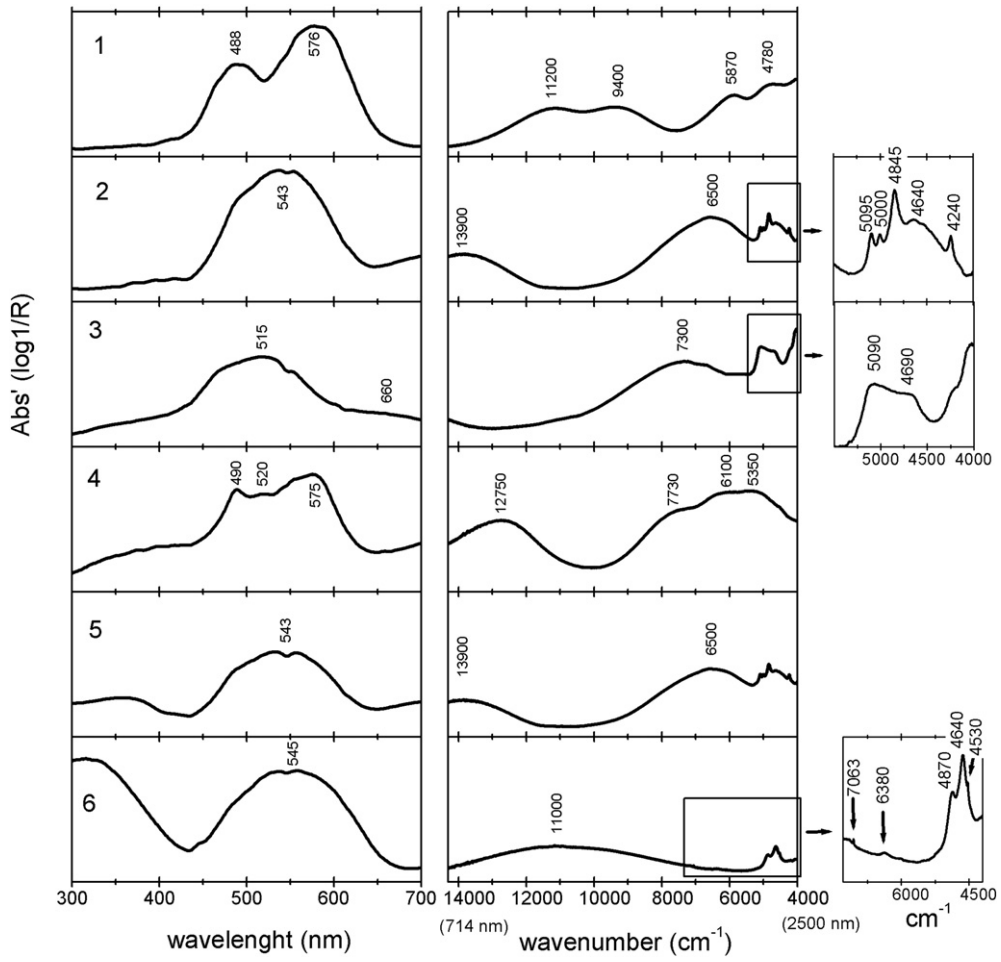

Fig. 3. UV–Vis (left column) and near-FTIR (right column) spectra of the investigated pigments. From Tables 1, **1** is $Co_3(PO_4)_2$, **2** $NH_4CoPO_4 \cdot H_2O$ from Kremer, **3** $Co_3(PO_4)_2 \cdot 8H_2O$, **4** $LiCoPO_4$, **5** $NH_4CoPO_4 \cdot H_2O$ (with $BaSO_4$) from Winsor & Newton, and **6** $NH_4MnP_2O_7$. Graphs on the right show a detailed view of the spectral profile for samples **2** (identical to **5**), **3** and **6** in the near infrared range evidenced by the solid boxes. For band assignment in the near infrared range see Table 3. Note that the recurrent depression at about 545 nm in the UV–Vis spectra (left column) is an instrumental artifact.

band splitting due to distortions of the octahedral geometry from the *Jahn-Teller* effect.

In the specific case of monoclinic cobalt phosphate - $Co_3(PO_4)_2$ (**1**) - electronic transitions are generated by cobalt ions in two different crystallographic sites: octahedral (six coordinated cobalt — Co(II)O6) and trigonal bipyramidal (five coordinated cobalt — Co(II)O5) [18]. The corresponding UV–Vis spectrum shows a distinct band at 576 nm which belongs to the Co(II)O6 configuration, being due to the $^4T_{1g} \rightarrow {}^4T_{1g}(P)$ transition, and a band at 488 nm arising from the $^4A_2 \rightarrow {}^4E(P)$ transition, belonging to Co(II)O5 [16,18].

The octahedral coordination of Co(II) in sample **2** (ammonium cobalt phosphate hydrate) is revealed by a broad band centered at 543 nm, matching exactly those of **5** from Winsor & Newton. Sample **3** (cobalt phosphate hydrate) exhibits a main band at 515 nm and a broad shoulder at about 660 nm (see band assignment in the next section); sample **4** (orthorhombic lithium cobalt phosphate) is characterized by a main absorption band at about 575 nm assigned to a $^4T_{1g}(F) \rightarrow {}^4T_{1g}(P)$ transition that is manifold splitted due to multiplet coupling [19].

Ammonium manganese pyrophosphate in sample **6** consists of Mn^{3+} ions in an octahedral configuration which, due to distortions of the coordination sphere, show the expected $^5E_g \rightarrow {}^5T_{2g}$ transition at about 545 nm [20,21]. This spectral feature in the UV–Vis range is not specific for pigment identification with respect to cobalt pigments, as, instead, it occurs in the near infrared region (see the next section).

3.2.2. NIR Electronic Spectral Range: 14,300–7000 cm^{-1}

In the 14,300-7000 cm^{-1} (700–1430 nm) spectral region, *d-d* transitions of the investigated compounds are still found. Sample **1** shows bands at about 11,200 cm^{-1} (893 nm) and 9400 cm^{-1} (1064 nm), 5870 cm^{-1} (1704 nm) and 4780 cm^{-1} (2092 nm); the 11,200 cm^{-1} one -belonging to Co(II)O5– corresponds to the $^4A_2 \rightarrow {}^4E$ transition, the 9400 cm^{-1} signal belongs to the octahedral configuration, being due to the $^4T_{1g} \rightarrow {}^4T_{2g}$ transition, while the one at 5870 cm^{-1} corresponds to the $^4A_2 \rightarrow {}^4E$ transition [18]. However a different band assignment has been recently proposed by Hunault and coworkers [16] which in consideration of the occurrence of another electronic band at 4780 cm^{-1} suggests the attribution of the observed electronic transitions to a strong distortion of the Co(II)O5 site towards C_{2v} symmetry generating a further splitting of the electronic levels.

Pigment **4** displays the $^4T_{1g} \rightarrow {}^4A_{2g}$ transition at about 12,750 cm^{-1} (784 nm) [19] while the same transition generates a band at about 13,900 cm^{-1} (719 nm) in samples **2** and **5**. In sample **3** we suggest as possible assignment for the $^4T_{1g} \rightarrow {}^4A_{2g}$ transition the shoulder at about 660 nm.

The broad band in the range around 7000 cm^{-1} in samples **2**, **3**, **4** and **5** is, instead, attributed to the $^4T_{1g} \rightarrow {}^4T_{2g}$ transition of octahedral Co(II) [17,22]. More in details, in samples **2** and **5** the broad band at 6500 cm^{-1} (1538 nm) contains both the contribution from the mentioned electronic transition and from the stretching overtones of H_2O and, possibly, of the ammonium ion [23,24]. This consideration is further supported by the mid-FTIR data of samples **2** and **5** (see Supplementary Material) where intense bending and stretching vibrational bands of both H_2O and of NH_4^+ ion are observed. Sample **3** shows the $^4T_{1g} \rightarrow {}^4T_{2g}$ electronic transition at 7300 cm^{-1} (1370 nm), while pigment **4** displays a band at 7730 cm^{-1} (1294 nm) [19].

In **6**, a distinctive *d-d* electronic transition due to the tetragonal distortion of the Mn^{3+} octahedral site is present at about 11,000 cm^{-1} (909 nm) [21].

3.2.3. NIR Vibrational Spectral Range: 7000–4000 cm^{-1}

Between 7000 and 4000 cm^{-1} (2500–1430 nm), where vibrational modes typically fall, phosphate minerals exhibit a large number of features; their complexity is mainly due to overtones and combination bands of water and, only for samples **2**, **5** and **6,** of the ammonium ion [23,25,26]. Different is the case of samples **1** and **4**, that being without O—H and N—H bonds show broad bands due to low energy *d-d* transitions at 5870 and 4780 cm^{-1} [16] and 6100 and 5350 cm^{-1}, respectively.

Pigments **2** and **5** (ammonium cobalt phosphate hydrate) have signals at around 5000 cm^{-1} (2000 nm) and 4845 cm^{-1} (2064 nm) due to combination modes of the ammonium ion, as reported in Table 3 [26]. The signal at 5095 cm^{-1} (1963 nm) comes from the combination of OH stretching and bending modes, while the broad electronic band at 6500 cm^{-1} (1540 nm) is convoluted with the spectral contribution from the overtone modes of both the crystallization water and the ammonium anion [23,24]. The sharp signal at 4240 cm^{-1} (2358 nm) in samples **2** and **5** has not been assigned and its interpretation still remains unclear.

In compound **3** the signals related to the combination of OH modes of crystallization water are at 5090 cm^{-1} (1965 nm) 'while the broad electronic band at 7300 cm^{-1} hinders the overtone modes of OH stretching. The origin of the band at 4690 cm^{-1} (2132 nm) is unclear and possibly ascribable to the combinations of $(PO_4)^{3-}$ modes [23].

In pigment **6** the signals at 4640 (2155 nm), 4870 cm^{-1} (2054 nm) and 6380 cm^{-1} (1567 nm) can tentatively be assigned to $\nu_1+\nu_4$, $\nu_2+\nu_3$ and $\nu_1+\nu_3$ combination bands of ammonium ion, respectively [26]. Kaolinite contributes with absorption bands at 4530 cm^{-1} and 7063 cm^{-1}.

3.3. Non-Invasive in situ Measurements on Paintings

During a MOLAB diagnostic campaign at the *Museo del Novecento* (Milano) some Boccioni's paintings have been analyzed: *Costruzione spiralica* 1913/14 (B5165), *Dinamismo di un corpo umano* 1913 (B5166), *Gli stati d'animo I –quelli che vanno* 1911 (B5174) and *Gli stati d'animo I –gli addii* 1911 (B5175).

XRF measurements on different violet areas showed the presence of cobalt in *Costruzione Spiralica* (B5165), and *Dinamismo di un corpo umano* (B5166), while Mn was found in the other two paintings. $Co_3(PO_4)_2$ was identified in B5165 and B5166, while Mn-violet was found in B5174 and B5175 by means of UV–Vis (Fig.4a and b) and near-FTIR spectroscopy (Fig.4c and d). This latter technique also identified an oil-based binder in B5174 and B5175 due to the observation of a doublet at about 4260 and 4340 cm^{-1} assigned to the combination of methylenic C—H stretching and bending modes (Fig. 5c) [27]. Although only near-FTIR spectroscopy was performed on the violet areas in B5166, XRD measurements could thoroughly confirmed anhydrous cobalt phosphate and also revealed hydrocerussite and gypsum (Fig. 5). It is worth to note that XRD analysis of real paintings can be hampered by several adverse factors which may limit crystalline phase detection. These include degree of crystallinity and grain size of the pigment, X-ray absorption matrix effects, co-presence of other high scattering pigments, and limited depth penetration of the X-ray beam. However, in case of positive results, XRD analysis provides an unambiguous confirmation of the spectroscopic data such as the case of the Boccioni's painting.

4. Conclusions

A complete, non-invasive characterization of some violet pigments as well as of some pure cobalt-containing violet salts, also known to be used by artists, was achieved by means of portable XRD, XRF, near-FTIR and UV–Vis instrumentation working in reflection directly on the pigment powders. The study was aimed at providing spectral reference standards of violet historical pigments for non-invasive investigation of paintings by the cited techniques. By near-FTIR and UV–Vis spectroscopy each pigment showed a different, peculiar spectrum which makes - after a mandatory elemental XRF analysis - its identification straightforward. An accurate XRD investigation performed both with portable and bench-top instruments allowed to reveal in 45350-"Manganviolett" from Kremer the presence of α-$NH_4MnP_2O_7$, as its main constituent,

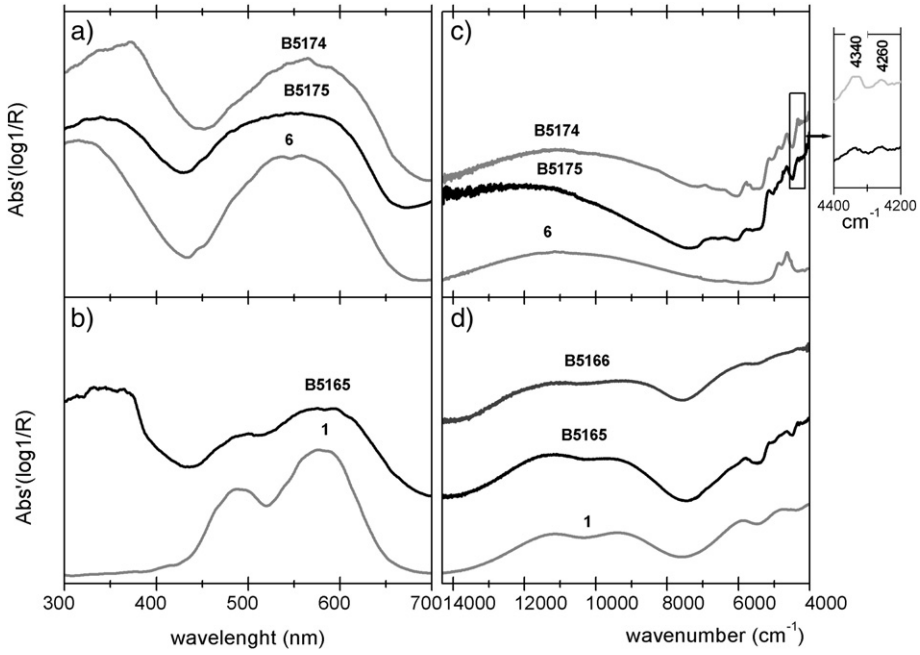

Fig. 4. a) and b) UV–Vis and c) and d) near-FTIR spectra of manganese violet standard (**6**) and cobalt phosphate standard (**1**) compared with collected *in situ* measurements on the Boccioni's paintings B5165, B5166, B5174, and B5175. Graph on the right shows a detailed view of the spectral profiles for B5174 and B5175 in the near infrared range evidenced by the solid box.

together with its β-phase, kaolinite and a small amount of stewartite. The presence of $Co_3(PO_4)_2$ and α-$NH_4MnP_2O_7$ on four Boccioni's paintings at the *Museo del Novecento* (Milano) was, then, ascertained by near-FTIR and UV–Vis analysis after XRF screening and supported by XRD measurements.

Supplementary data to this article can be found online at http://dx.doi.org/10.1016/j.saa.2016.09.017.

Acknowledgments

We gratefully acknowledge for financial support of the national research projects SICH (PRIN 2010–2011 program) (2010329WPF) and FUTURAHMA (Future in Research - 2012 program) (RBFR12PHL4), both funded by the Italian Ministry of Education, University and Research (MIUR). The authors are also grateful to the Museo del Novecento to have made possible the MOLAB campaign.

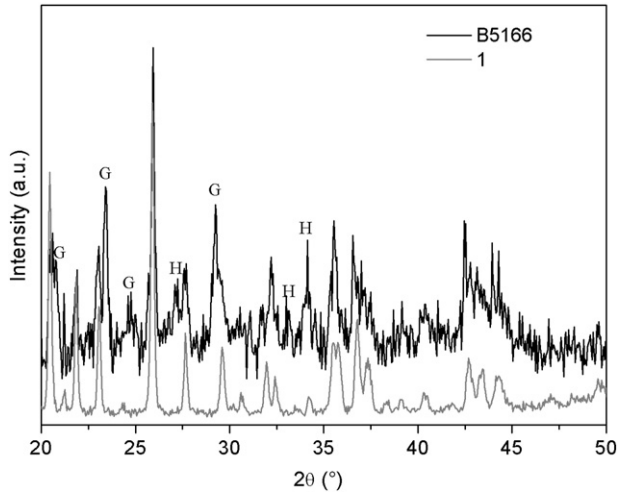

Fig. 5. XRD pattern collected on a violet area in painting B5166 (H = hydrocerusite, G = gypsum) compared with the diffractogram of pigment **1**.

References

[1] Project FUTURAHMA (2013–2016) of the Future in Research 2012 program founded by MIUR (http://www.futurahma.it/en/home/).
[2] M.C. Corbeil, J.P. Charland, E.A. Moffat, Stud. Conserv. 47 (2002) 237–249.
[3] R.J. Gettens, G.L. Stout, Painting Materials: A Short Encyclopaedia, Dover Publication, New York, 1966.
[4] N. Eastaugh, V. Walsh, T. Chaplin, R. Siddall, Pigment Compendium: A Dictionary and Optical Microscopy of Historical Pigments, Butterworth-Heinemann, Oxford, UK, 2004.
[5] R. Jonynaitė, D. Senvaitienė, J. Kiuberis, J. Kareiva, A. Juškėnas, R. Ramanauskas, R. Chemija 20 (2009) 10–18.
[6] F. Casadio, A. Bezúr, I. Fiedler, K. Muir, T. Trad, S. Maccagnola, J. Raman, Spectrosc. 43 (2012) 1761–1771.
[7] C. Miliani, F. Rosi, G. Brunetti, A. Sgamellotti, Acc. Chem. Res. 43 (2010) 728–738.
[8] A. Duran, J.L. Perez-Rodriguez, T. Espejo, M.L. Franquelo, J. Castaing, P. Walter, Anal. Bioanal. Chem. 395 (2009) 1997–2004.
[9] G. Chiari, Nature 458 (2008) 159.
[10] P. Sarrazin, G. Chiari, M. Gailhanou, Adv. X-ray Anal. 52 (2008) 175–186.
[11] C. Larson, R.B. von Dreele, Generalized Crystal Structure Analysis System, Los Alamos National Laboratory, Los Alamos, NM, 2001.
[12] A. Romani, C. Grazia, C. Anselmi, C. Miliani, B.G. Brunetti, New portable instrument for combined reflectance, time-resolved and steady-state luminescence measurements on works of art, Proc. SPIE 8084 (2011) 808403, http://dx.doi.org/10.1117/12.889529.
[13] Z. Chen, Q. Chai, S. Liao, Y. He, Y. Li, X. Bo, W. Wu, B. Li, Thermochim. Acta 543 (2012) 205–210.
[14] T. Mimani, S. Ghosh, Curr. Sci. 78 (2000) 892–896.
[15] M. Bacci, M. Picollo, Stud. Conserv. 41 (1996) 136–144.
[16] M. Hunault, J.-L. Robert, M. Newville, L. Galoisy, G. Calas, Spectrochim. Acta A Mol. Biomol. Spectrosc. 117 (2014) 406–412.
[17] M. Llusar, A. Zielinska, M.A. Tena, J.A. Badenes, G. Monrós, J. Eur. Ceram. Soc. 30 (2010) 1887–1896.
[18] S. Meseguer, M.A. Tena, G. Gargori, J.A. Badenes, M. Llusar, G. Monrós, Ceram. Int. 33 (2007) 843–849.
[19] M. Gaudon, P. Deniard, L. Voisin, G. Lacombe, F. Darnat, A. Demourgues, J.-L. Perillon, S. Jobic, Dyes Pigments 95 (2012) 344–350.
[20] Y. Begum, A.J. Wright, J. Mater. Chem. 22 (2012) 21110–21116.
[21] D.M. Sherman, N. Vergo, Am. Mineral. 73 (1988) 140–144.
[22] Q. Tao, B.J. Reddy, H. He, R.L. Frost, P. Yuana, J. Zhu, Mater. Chem. Phys. 112 (2008) 869–875.
[23] R.L. Frost, B.J. Reddy, S.J. Palmer, E.C. Keeffe, Spectrochim. Acta A 78 (2011) 996–1003.
[24] G.R. Hunt, Geophysics 42 (1977) 501–513.
[25] R.L. Frost, B.J. Reddy, E.C. Keeffe, Transit. Met. Chem. 35 (2010) 667–678.
[26] M.D. Krohn, S.P. Altaner, Geophysics 52 (1987) 924–930.
[27] M. Vagnini, C. Miliani, L. Cartechini, P. Rocchi, B.G. Brunetti, A. Sgamellotti, Anal. Bioanal. Chem. 395 (2009) 2107–2118.